

# Chapter 7

## High Order SFV and Mixed SDG/FV Methods for the Uncertainty Quantification in Multidimensional Conservation Laws

Svetlana Tokareva, Christoph Schwab, and Siddhartha Mishra

**Abstract** We analyze and apply the high order Stochastic Finite Volume (SFV) and mixed Stochastic Discontinuous Galerkin/Finite Volume (SDG/FV) methods used to quantify the uncertainty in hyperbolic conservation laws with random initial data and flux coefficients. We describe incomplete information in the conservation law mathematically as random fields. The SFVM is formulated to solve numerically the system of conservation laws with sources of randomness in both flux coefficients and initial data. We formulate the Stochastic Discontinuous Galerkin method which we primarily use to solve the multidimensional stochastic conservation laws on unstructured grids. Finally, we compare the efficiency of the SFV and SDG methods with of Monte-Carlo type methods. Finally, we introduce an adaptation technique based on the Karhunen-Loève expansion of the random flux and/or initial data and apply it in order to reduce the computational cost of the SFVM.

### 7.1 Introduction

We analyze and apply the high order Stochastic Finite Volume method (SFVM) [1–3, 20] and mixed Stochastic Discontinuous Galerkin/Finite Volume (SDG/FV) methods used to quantify the uncertainty in hyperbolic conservation laws with random initial data and flux coefficients. The direct application of these methods

---

S. Tokareva (✉)  
ASCOMP GmbH, Zurich, Switzerland

Seminar for Applied Mathematics, ETH Zurich, Zurich, Switzerland  
e-mail: [tokareva@ascomp.ch](mailto:tokareva@ascomp.ch)

C. Schwab • S. Mishra  
Seminar for Applied Mathematics, ETH Zurich, Zurich, Switzerland

is the simulation of gas flows with uncertain physical parameters and/or initial flow conditions. Many efficient numerical methods have been developed to approximate the entropy solutions of systems of conservation laws [7], however, in many practical applications it is not always possible to obtain exact physical data due to, for example, measurement or modeling errors. We describe incomplete information in the conservation law mathematically as random fields. Such data are described in terms of statistical quantities of interest like the mean, variance, higher statistical moments; in some cases the distribution law of the stochastic initial data is also assumed to be known. There exist several techniques to quantify the uncertainty (i.e. determine the mean flow and its statistical moments), such as the Monte-Carlo (MC), the Multi-Level Monte Carlo (MLMC) and Stochastic Galerkin method (see also [5, 8–15, 19, 22–26]). The SFVM is formulated to solve numerically the system of conservation laws with sources of randomness in both flux coefficients and initial data. We generalize this approach and formulate the Stochastic Discontinuous Galerkin method which we primarily use to solve the multidimensional stochastic conservation laws on unstructured grids. Finally, we compare the efficiency of the SFV and SDG methods with of Monte-Carlo type methods. Finally, we introduce an adaptation technique based on the Karhunen-Loève expansion of the random flux and/or initial data and apply it in order to reduce the computational cost of the SFVM.

## 7.2 Conservation Laws with Random Flux and Initial Data

Consider the hyperbolic system of conservation laws with random flux coefficients

$$\partial_t \mathbf{U} + \nabla_x \cdot \mathbf{F}(\mathbf{U}, \omega) = \mathbf{0}, \quad t > 0; \quad (7.1)$$

$\mathbf{x} = (x_1, x_2, x_3) \in D_x \subset \mathbb{R}^3$ ,  $\mathbf{U} = [u_1, \dots, u_p]^T$ ,  $\mathbf{F} = [\mathbf{F}_1, \mathbf{F}_2, \mathbf{F}_3]$ ,  $\mathbf{F}_k = [f_1, \dots, f_p]^T$ ,  $k = 1, 2, 3$ , and random initial data

$$\mathbf{U}(\mathbf{x}, 0, \omega) = \mathbf{U}_0(\mathbf{x}, \omega), \quad \omega \in \Omega. \quad (7.2)$$

A mathematical framework of *random entropy solutions* for scalar conservation laws has been developed in [16]. There, existence and uniqueness of random entropy solutions to (7.1)–(7.2) has been shown for scalar hyperbolic conservation laws, also in multiple dimensions. Furthermore, the existence of the statistical quantities of the random entropy solution such as the statistical mean and  $k$ -point spatio-temporal correlation functions under suitable assumptions on the random initial data have been proven.

### 7.3 Stochastic FVM

We parametrize all the random inputs in the Eqs.(7.1)–(7.2) using the random variable  $\mathbf{y} = \mathbf{Y}(\omega)$  which takes values in  $D_y \subset \mathbb{R}^q$  and rewrite the stochastic conservation law in the parametric form:

$$\partial_t \mathbf{U} + \nabla_x \cdot \mathbf{F}(\mathbf{U}, \mathbf{y}) = \mathbf{0}, \quad \mathbf{x} \in D_x \subset \mathbb{R}^3, \quad \mathbf{y} \in D_y \subset \mathbb{R}^q, \quad t > 0; \quad (7.3)$$

$$\mathbf{U}(\mathbf{x}, 0, \mathbf{y}) = \mathbf{U}_0(\mathbf{x}, \mathbf{y}), \quad \mathbf{x} \in D_x \subset \mathbb{R}^3, \quad \mathbf{y} \in D_y \subset \mathbb{R}^q. \quad (7.4)$$

Let  $\mathcal{T}_x = \cup_{i=1}^{N_x} K_x^i$  be the triangulation of the computational domain  $D_x$  in the physical space and  $\mathcal{C}_y = \cup_{j=1}^{N_y} K_y^j$  be the Cartesian grid in the domain  $D_y$  of the parametrized probability space.

We further assume the existence of the probability density function  $\mu(\mathbf{y})$  and compute the expectation of the  $n$ -th solution component of the conservation law (7.3)–(7.4) as follows:

$$\mathbb{E}[u_n] = \int_{D_y} u_n \mu(\mathbf{y}) d\mathbf{y}, \quad n = 1, \dots, p$$

The scheme of the Stochastic Finite Volume method (SFVM) [1–3] can be obtained from the integral form of the Eqs. (7.3)–(7.4):

$$\iint_{K_y^j K_x^i} \partial_t \mathbf{U} \mu(\mathbf{y}) d\mathbf{x} d\mathbf{y} + \iint_{K_y^j K_x^i} \nabla_x \cdot \mathbf{F}(\mathbf{U}, \mathbf{y}) \mu(\mathbf{y}) d\mathbf{x} d\mathbf{y} = \mathbf{0}.$$

Introducing the cell average

$$\bar{\mathbf{U}}_{ij}(t) = \frac{1}{|K_x^i| |K_y^j|} \iint_{K_y^j K_x^i} \mathbf{U}(\mathbf{x}, t, \mathbf{y}) \mu(\mathbf{y}) d\mathbf{x} d\mathbf{y}$$

with the cell volumes

$$|K_x^i| = \int_{K_x^i} d\mathbf{x}, \quad |K_y^j| = \int_{K_y^j} \mu(\mathbf{y}) d\mathbf{y}$$

and performing the partial integration over  $K_x^i$  we get

$$\frac{d\bar{\mathbf{U}}_{ij}}{dt} + \frac{1}{|K_x^i| |K_y^j|} \int_{K_y^j} \left[ \int_{K_x^i} \mathbf{F}(\mathbf{U}, \mathbf{y}) \cdot \mathbf{n} dS \right] \mu(\mathbf{y}) d\mathbf{y} = \mathbf{0}$$

Next, we use any standard numerical flux approximation  $\hat{\mathbf{F}}(\bar{\mathbf{U}}_L(\mathbf{x}, t, \mathbf{y}), \bar{\mathbf{U}}_R(\mathbf{x}, t, \mathbf{y}), \mathbf{y})$  to replace the discontinuous flux through the element interface  $\mathbf{F}(\mathbf{U}, \mathbf{y}) \cdot \mathbf{n}$ .

Here  $\tilde{\mathbf{U}}_{L,R}$  denote the boundary extrapolated solution values at the edge of the cell  $K_x^i$ , obtained by the high order reconstruction from the cell averages. The complete numerical flux is then approximated by a suitable quadrature rule as

$$\bar{\mathbf{F}}_{ij}(t) = \frac{1}{|K_y^j|} \int_{K_y^j} \left[ \int_{K_x^i} \hat{\mathbf{F}}(\tilde{\mathbf{U}}_L, \tilde{\mathbf{U}}_R, \mathbf{y}) \right] \mu(\mathbf{y}) d\mathbf{y} \approx \frac{1}{|K_y^j|} \sum_{\mathbf{m}} \hat{\mathcal{F}}(t, \mathbf{y}_{\mathbf{m}}) \mu(\mathbf{y}_{\mathbf{m}}) w_{\mathbf{m}}, \quad (7.5)$$

where we have denoted the flux integral over the physical cell as  $\hat{\mathcal{F}}$ ,  $\mathbf{m} = (m_1, \dots, m_q)$  is the multi-index,  $\mathbf{y}_{\mathbf{m}}$  and  $w_{\mathbf{m}}$  are quadrature nodes and weights, respectively.

The SFV method then results in the solution of the following ODE system:

$$\frac{d\tilde{\mathbf{U}}_{ij}}{dt} + \frac{1}{|K_x^i|} \bar{\mathbf{F}}_{ij}(t) = \mathbf{0}, \quad (7.6)$$

for all  $i = 1, \dots, N_x$ ,  $j = 1, \dots, N_y$ . Therefore, to obtain the high-order scheme we first need to provide the high-order flux approximation based, for example, on the ENO/WENO reconstruction in the physical space. Second, we have to guarantee the high-order integration in (7.5) also by applying the ENO/WENO reconstruction in the stochastic space and choosing the suitable quadrature rule. Finally, we need the high-order time-stepping algorithm to solve the ODE system (7.6), such as Runge-Kutta method.

## 7.4 Convergence and Efficiency Analysis for SFVM

In this section we present the results of the convergence and efficiency analysis of the SFV method applied to the stochastic scalar conservation law in the parametric form

$$\partial_t u + \partial_x f(u; y) = 0, \quad x \in D, \quad y \in Y, \quad t > 0, \quad (7.7)$$

$$u(x, 0; y) = u_0(x; y). \quad (7.8)$$

Let  $Y = \bigcup_{k=1}^{N_y} Y_k$ , where  $Y_k$  is the mesh cell in the stochastic variable  $y$ . Denote the probability density function by  $\mu(y)$ .

### 7.4.1 Convergence of Statistical Moments in $L^1$ -Norm

Denote by  $u$  the exact solution of (7.7), by  $u_h^y$  the numerical solution which is exact in  $x$  variable and discretized in  $y$  and by  $u_h^{xy}$  the numerical discretized in both

variables. Assume that the numerical solution converges with rate  $p$  in  $x$  variable and rate  $r$  in  $y$  variable, that is

$$\|u_h^y - u_h^{xy}\|_{L^1(D)} \leq C_1 \Delta x^p \quad \forall y \in Y. \quad (7.9)$$

$$\|u - u_h^y\|_{L^1(Y)} \leq C_2 \Delta y^r \quad \forall x \in D, \quad (7.10)$$

The next estimate follows immediately from this assumption:

$$\|u - u_h^{xy}\|_{L^1(D \times Y)} \leq C_1 \Delta x^p + C_2 \Delta y^r. \quad (7.11)$$

**Convergence of  $E_h[u_h^{xy}]$  in  $L^1$ -norm** The expected value of the exact solution is a deterministic function

$$\mathbb{E}[u](x_i, t^n) = \int_Y u(x_i, t^n; y) \mu(y) dy, \quad (7.12)$$

and the approximation of the expectation of the numerical solution is, as before, equal to

$$E_h[u_h^{xy}]_i^n = \sum_{k=1}^{N_y} u_{ik}^n \omega_k = \sum_{k=1}^{N_y} u_{ik}^n \int_{Y_k} \mu(y) dy = \sum_{k=1}^{N_y} \int_{Y_k} u_{ik}^n \mu(y) dy = \mathbb{E}[u_h^{xy}](x_i, t^n). \quad (7.13)$$

Then

$$\begin{aligned} \|\mathbb{E}[u] - \mathbb{E}[u_h^{xy}]\|_{L^1(D)} &= \|\mathbb{E}[u] - \mathbb{E}[u_h^y] + \mathbb{E}[u_h^y] - \mathbb{E}[u_h^{xy}]\|_{L^1(D)} \leq \\ &\leq \|\mathbb{E}[u] - \mathbb{E}[u_h^y]\|_{L^1(D)} + \|\mathbb{E}[u_h^y] - \mathbb{E}[u_h^{xy}]\|_{L^1(D)} = \\ &= \int_D |\mathbb{E}[u] - \mathbb{E}[u_h^y]| dx + \int_D |\mathbb{E}[u_h^y] - \mathbb{E}[u_h^{xy}]| dx = \\ &= \int_D \left| \int_Y (u - u_h^y) \mu(y) dy \right| dx + \int_D \left| \int_Y (u_h^y - u_h^{xy}) \mu(y) dy \right| dx \leq \\ &\leq \int_D \int_Y |u - u_h^y| \mu(y) dy dx + \int_D \int_Y |u_h^y - u_h^{xy}| \mu(y) dy dx. \end{aligned} \quad (7.14)$$

The first integral in (7.14) can be estimated as follows:

$$\int_D \int_Y |u - u_h^y| \mu(y) dy dx \leq \int_D \sup_Y \mu(y) \int_Y |u - u_h^y| dy dx = C \|u - u_h^y\|_{L^1(Y)} \leq C \Delta y^r, \quad (7.15)$$

and for the second integral we have

$$\begin{aligned} \int_D \int_Y |u_h^y - u_h^{xy}| \mu(y) dy dx &= \int_Y \left[ \int_D |u_h^y - u_h^{xy}| dx \right] \mu(y) dy = \\ &= \|u_h^y - u_h^{xy}\|_{L^1(D)} \int_Y \mu(y) dy = \|u_h^y - u_h^{xy}\|_{L^1(D)} \leq C \Delta x^p. \end{aligned} \quad (7.16)$$

Hence, the convergence rate of the expectation in  $L^1$ -norm can be estimated as

$$\|\mathbb{E}[u] - \mathbb{E}[u_h^{xy}]\|_{L^1(D)} \leq C_1 \Delta x^p + C_2 \Delta y^r. \quad (7.17)$$

**Convergence of  $V_h[u_h^{xy}]$  in  $L^1$ -norm** The variance of the exact solution at  $(x_i, t^n)$  is equal to

$$\mathbb{V}[u](x_i, t^n) = \mathbb{E}[(u(x_i, t^n) - \mathbb{E}[u](x_i, t^n))^2] = \mathbb{E}[u^2(x_i, t^n)] - (\mathbb{E}[u](x_i, t^n))^2, \quad (7.18)$$

and can be approximated as

$$V_h[u_h^{xy}]_i^n = E_h[(u_h^{xy})^2]_i^n - (E_h[u_h^{xy}]_i^n)^2 = \mathbb{E}[(u_h^{xy})^2]_i^n - (\mathbb{E}[u_h^{xy}]_i^n)^2 = \mathbb{V}[u_h^{xy}]_i^n. \quad (7.19)$$

Then

$$\begin{aligned} \|\mathbb{V}[u] - \mathbb{V}[u_h^{xy}]\|_{L^1(D)} &= \|\mathbb{E}[u^2] - (\mathbb{E}[u])^2 - \mathbb{E}[(u_h^{xy})^2] + (\mathbb{E}[u_h^{xy}])^2\|_{L^1(D)} \leq \\ &\leq \|\mathbb{E}[u^2] - \mathbb{E}[(u_h^{xy})^2]\|_{L^1(D)} + \|(\mathbb{E}[u])^2 - (\mathbb{E}[u_h^{xy}])^2\|_{L^1(D)}. \end{aligned} \quad (7.20)$$

The following estimate holds for the first integral in (7.20):

$$\begin{aligned} \|\mathbb{E}[u^2] - \mathbb{E}[(u_h^{xy})^2]\|_{L^1(D)} &= \int_D |\mathbb{E}[u^2] - \mathbb{E}[(u_h^{xy})^2]| dx = \\ &= \int_D \left| \int_Y [u^2 - (u_h^{xy})^2] \mu(y) dy \right| dx \leq \int_D \int_Y |u^2 - (u_h^{xy})^2| \mu(y) dy dx = \\ &= \int_D \int_Y |u - u_h^{xy}| |u + u_h^{xy}| \mu(y) dy dx \leq C \int_D \int_Y |u - u_h^{xy}| dy dx = \\ &= C \|u - u_h^{xy}\|_{L^1(D \times Y)} \leq C \Delta x^p + C_7 \Delta y^r. \end{aligned} \quad (7.21)$$

For the second integral in (7.20) we get

$$\begin{aligned} \left\| (\mathbb{E}[u])^2 - (\mathbb{E}[u_h^{xy}])^2 \right\|_{L^1(D)} &= \int_D |(\mathbb{E}[u])^2 - (\mathbb{E}[u_h^{xy}])^2| dx = \\ &= \int_D |\mathbb{E}[u] - \mathbb{E}[u_h^{xy}]| |\mathbb{E}[u] + \mathbb{E}[u_h^{xy}]| dx \leq \\ &\leq C \left\| \mathbb{E}[u] - \mathbb{E}[u_h^{xy}] \right\|_{L^1(D)} \leq C_1 \Delta x^p + C_2 \Delta y^r. \end{aligned} \quad (7.22)$$

Finally, from (7.21) to (7.22) we get

$$\left\| \mathbb{V}[u] - \mathbb{V}[u_h^{xy}] \right\|_{L^1(D)} \leq C_1 \Delta x^p + C_2 \Delta y^r. \quad (7.23)$$

Similar estimates are also valid for higher moments of  $u$ .

## 7.4.2 Efficiency Estimates

In the previous section it has been shown that the error of the expectation approximation is given by

$$E = \left\| \mathbb{E}[u] - \mathbb{E}[u_h^{xy}] \right\|_{L^1(D)} \leq C_1 \Delta x^p + C_2 \Delta y^r, \quad (7.24)$$

where  $p$  and  $r$  are the convergence rates of the SFVM solver in physical and stochastic variables, respectively. Based on this result, we derive the error vs. work estimates for SFVM.

Let  $x \in \mathbb{R}^n$ ,  $y \in \mathbb{R}^m$ . Assume that the CFL condition is satisfied, such that  $\Delta t = O(\delta x)$ . The total work  $W$  (or total time) required to compute the solution of the stochastic scalar conservation law using SFVM is proportional to the total numbers of grid points in  $x$ ,  $y$  and  $t$  axes, denoted respectively by  $N_x$ ,  $N_y$  and  $N_t$ , i.e.

$$W = CN_x N_y N_t = C \frac{1}{\Delta x^n} \frac{1}{\Delta y^m} \frac{1}{\Delta t} = \frac{C}{\Delta x^{n+1} \Delta y^m} = C \Delta x^{-(n+1)} \Delta y^{-m}. \quad (7.25)$$

Further derivation of the estimate depends on the choice of the mesh sizes equilibration, that is, on the relation between  $\Delta x$  and  $\Delta y$ .

1. Assume that the mesh sizes are equilibrated according to the expected orders of convergence  $p$  and  $r$ :  $\Delta y = \Delta x^{p/r}$ . Then  $E = C \Delta x^p$  and  $\Delta x = CE^{1/p}$ . Substituting these relations into the Eq. (7.25) we get

$$W = C \Delta x^{-(n+1)} \Delta x^{-pm/r} = C \Delta x^{-(n+1+pm/r)} = CE^{-\frac{n+1+pm/r}{p}} \quad (7.26)$$

and hence

$$E = CW^{-\frac{p}{n+1+pm/r}}, \quad (7.27)$$

which is the desired error vs. work estimated.

2. Assume now that the mesh size  $\Delta y$  is obtained by the following scaling:  $\Delta y = \eta \Delta x$ , where  $\eta$  is the constant scaling factor, meaning that the stochastic mesh is isotropic (same  $\Delta y$  for all random variables). Define  $q = \min(p, r)$ . Then  $E = C \Delta x^q$  and  $\Delta x = CE^{1/q}$ , and the total work is defined as

$$W = C \Delta x^{-(n+1)} \Delta y^{-m} = C \Delta x^{-(n+m+1)} = CE^{-\frac{n+m+1}{q}}, \quad (7.28)$$

which finally gives

$$E = CW^{-\frac{q}{n+m+1}}. \quad (7.29)$$

Note that the estimate (7.29) is equivalent to the complexity result for the deterministic finite-volume method in the  $(n + m)$ -dimensional space, which sets strict limitations on the number of random variables that can be handled by the SFVM if the scaling factor  $\eta$  is close to 1. However, computational practice shows that it is sufficient to use only few computational cells to discretize the equations in the stochastic space to obtain a good quality approximation of the statistical quantities and therefore the SFVM is essentially much more efficient as deterministic FVM. Another significant simplification of the approach is the absence of the fluxes in the stochastic variables  $y$ , which also contributes to the efficiency of the SFVM.

3. Assume that the stochastic mesh is anisotropic, that is the mesh sizes  $\Delta y_k$  are different for  $k = 1, \dots, m$ :  $\Delta y_k = \eta_k \Delta x$ . Applying the same technique as above we obtain

$$E = C_1 \Delta x + C_2 \sum_{k=1}^m \Delta y_k^r = C_1 \Delta x + C_2 \Delta x^r \sum_{k=1}^m \eta_k^r \leq C \Delta x^q \left(1 + \sum_{k=1}^m \eta_k^r\right), \quad (7.30)$$

where  $q = \min(p, r)$  as before. We have also assumed that  $\Delta x \ll 1$  such that  $\Delta x^p < \Delta x^q$  and  $\Delta x^r < \Delta x^q$ . Then the mesh size  $\Delta x$  can be represented as

$$\Delta x = \left( \frac{E}{1 + \sum_{k=1}^m \eta_k^r} \right)^{1/q}. \quad (7.31)$$



The total work is

$$W = C \left( \prod_{k=1}^m \eta_k^{-1} \right) \Delta x^{-(n+m+1)} = C \left( \prod_{k=1}^m \eta_k^{-1} \right) \left( \frac{E}{1 + \sum_{k=1}^m \eta_k^r} \right)^{-(n+m+1)/q}, \quad (7.32)$$

and the resulting error vs. work estimate is

$$E = C \left( 1 + \sum_{k=1}^m \eta_k^r \right) \left( \prod_{k=1}^m \eta_k^{-\frac{q}{n+m+1}} \right) W^{-\frac{q}{n+m+1}}. \quad (7.33)$$

Note that in the isotropic case, when all  $\eta_k = \eta = \text{const}$ , formula (7.33) results in

$$E = C(1 + m\eta^r) \eta^{-\frac{qm}{n+m+1}} W^{-\frac{q}{n+m+1}}. \quad (7.34)$$

Comparing (7.33) and (7.34) we notice that the proper choice of scaling factors  $\eta_k$  in the anisotropic stochastic mesh construction, while not affecting the convergence *rates*, can reduce the convergence constant, which means increasing computational efficiency. The choice of  $\eta_k$  should be based on the sensitivity analysis of the random entropy solution to each of the  $m$  random variables.

Let us demonstrate the efficiency provided by the anisotropic mesh adaptation. We compare the convergence constants:

$$C_i = (1 + m\eta^r) \eta^{-\frac{qm}{n+m+1}} \quad (7.35)$$

for the *isotropic* mesh with equal mesh sizes in all stochastic coordinates,  $\Delta y_k = \eta \Delta x$ ,  $k = 1, \dots, m$ , and

$$C_a = \left( 1 + \sum_{k=1}^m \eta_k^r \right) \prod_{k=1}^m \eta_k^{-\frac{q}{n+m+1}} \quad (7.36)$$

for the *anisotropic* stochastic mesh with mesh size scaling according to  $\Delta y_k = \eta_k \Delta x$ ,  $k = 1, \dots, m$ . Assume further that  $\eta_1 > \eta_2 > \dots > \eta_m$  and  $\eta_k > 1$  for all  $k$ , such that  $\Delta y_k > \Delta x$ .

Our goal is to show that the convergence constants ratio  $\delta_m = \frac{C_i}{C_a} > 1$  as  $m \rightarrow \infty$  if  $\eta_1 < \eta$  and  $r > q$ , that is, the anisotropic stochastic mesh increases the algorithm efficiency as the number of random variables grows if the convergence rate  $r$  in the stochastic space is higher than  $q$ , the minimum of the convergence rates in physical and stochastic coordinates.

We start by noting that under the assumption  $\eta_1 < \eta$  the following inequality is valid:

$$C_a = \left(1 + \sum_{k=1}^m \eta_k^r\right) \prod_{k=1}^m \eta_k^{-\frac{q}{n+m+1}} < (1 + m\eta_1^r) \eta_1^{-\frac{qm}{n+m+1}} = C_a^1, \quad (7.37)$$

and therefore

$$\delta_m = \frac{C_i}{C_a} > \frac{C_i}{C_a^1} = \frac{(1 + m\eta^r) \eta^{-\frac{qm}{n+m+1}}}{(1 + m\eta_1^r) \eta_1^{-\frac{qm}{n+m+1}}} = \left(\frac{1 + m\eta^r}{1 + m\eta_1^r}\right) \left(\frac{\eta}{\eta_1}\right)^{-\frac{qm}{n+m+1}}. \quad (7.38)$$

Hence, the limit of the constants ratio is

$$\delta = \lim_{m \rightarrow \infty} \delta_m = \left(\frac{\eta}{\eta_1}\right)^{r-q}, \quad (7.39)$$

and clearly  $\delta > 1$  if  $r > q$ .

Let's analyse in more detail the possible values of  $\delta$  in dependence on the convergence rates  $p$  and  $r$  in  $x$  and  $y$  variables, respectively.

**Smooth solution.** If the solution is smooth in  $x$  and  $y$ , then the convergence rate of the SFVM is the expected one, therefore by applying high-order finite-volume approximations in both variables one can obtain the full convergence rates  $p$  and  $r$ .

- If  $p < r$ , then  $q = \min(p, r) = p$  and  $r - q = r - p > 0$ ,  $\delta > 1$  and hence the SFVM will converge faster on anisotropic stochastic mesh.
- If  $p > r$ , then  $q = \min(p, r) = r$  and  $r - q = r - r = 0$ ,  $\delta = 1$ , therefore the anisotropic mesh doesn't improve the convergence.

**Shock solution.** Recall that if the shock wave appears in the physical space, then it also propagates into the stochastic space, so that the solution becomes discontinuous in both  $x$  and  $y$ . In this case the 1st order FV scheme one typically gives  $p = 1/2$  according to and  $r = 1$  as shown in [18], therefore  $q = \min(p, r) = 1/2$  and  $\delta = \sqrt{\frac{\eta}{\eta_1}} > 1$ . This means that the SFVM on anisotropic mesh in the stochastic space is more efficient than SFVM on the uniform mesh even if the solution has a shock.

### 7.4.3 Numerical Convergence Analysis

We perform the convergence analysis of the SFVM for a simple linear advection equation with uncertain phase initial condition

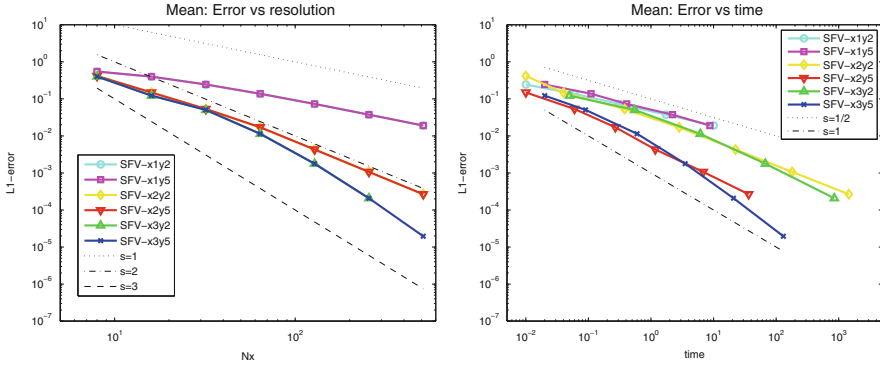


**Fig. 7.1** Mean: dependence of the error on the mesh resolution and computational time

$$u_t + au_x = 0, \quad x \in (0, 1),$$

$$u(x, 0) = \sin(2\pi(x + 0.1Y(\omega))).$$

The random variable  $y = Y(\omega)$  is assumed to be distributed uniformly on  $[0, 1]$ .

In Figs. 7.1–7.2, we plot the  $L^1(0, 1)$  error for the expectation and the variance of  $u$  with respect to the mesh size and the computational time. We investigate the influence of different reconstruction orders in spacial and stochastic variables on the convergence rates and therefore present the convergence plots for the SFVM based on different combinations of ENO/WENO reconstruction in  $x$  and  $y$ . We compare the SFVM with 1st, 2nd and 3rd order of accuracy in physical space combined with 3rd and 5th order reconstruction in stochastic variable. The type of reconstruction is indicated in Figs. 7.1–7.2 as follows: for example, the line “SFV-x2y5” corresponds to the 2nd order piecewise-linear ENO reconstruction in  $x$  and 5th order piecewise-quadratic WENO reconstruction in  $y$ , the line “SFV-x3y5” stands for 3rd order piecewise-linear WENO reconstruction in  $x$  with 5th order WENO reconstruction in  $y$ , etc. The numerical flux used in all the numerical experiments of this paper is the Rusanov flux. The results show that, while the convergence rate is dominated by the order of accuracy in  $x$ , the algorithms with higher order reconstruction in  $y$  are more efficient computationally since the same error can be reached with less overall computational time as compared to the lower order reconstruction in  $y$ .

### 7.4.4 Numerical Results

#### 7.4.4.1 Stochastic Sod’s Shock Tube Problem

Consider the Riemann problem for the one-dimensional Euler equations with randomness in both flux and initial data

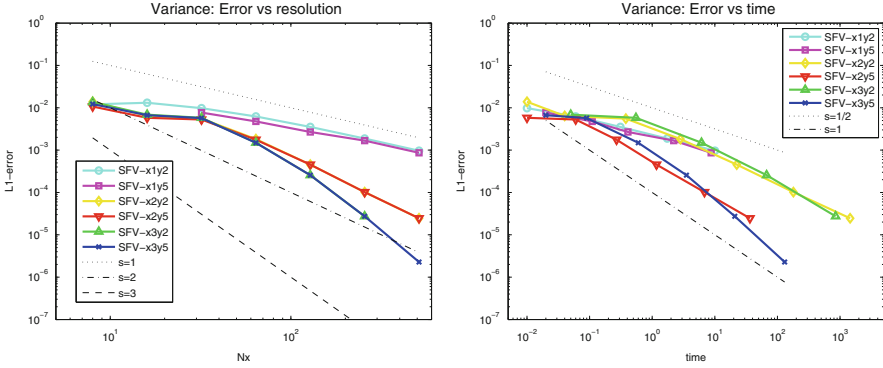


**Fig. 7.2** Variance: dependence of the error on the mesh resolution and computational time

$$\frac{\partial \mathbf{U}}{\partial t} + \frac{\partial \mathbf{F}(\mathbf{U}, \omega)}{\partial x} = \mathbf{0}, \quad x \in (0, 2), \quad (7.40)$$

$$\mathbf{U}(x, 0, \omega) = \mathbf{U}_0(x, Y_1(\omega), Y_2(\omega)) = \begin{cases} \mathbf{U}_L(Y_2(\omega)), & x < Y_1(\omega); \\ \mathbf{U}_R, & x > Y_1(\omega), \end{cases} \quad (7.41)$$

with  $y_j = Y_j(\omega)$ ,  $j = 1, 2, 3$ ,  $\omega \in \Omega$  and

$$\mathbf{U} = [\rho, \rho u, E]^T, \quad \mathbf{F} = [\rho u, \rho u^2 + p, \rho u(E + p)]^T,$$

$$p = (\gamma - 1) \left( E - \frac{1}{2} \rho u^2 \right).$$

We also assume the randomness in the adiabatic constant,  $\gamma = \gamma(Y_3(\omega))$ , and therefore

$$\mathbf{F}(\mathbf{U}, \omega) = \mathbf{F}(\mathbf{U}, Y_3(\omega)).$$

The initial data is set in primitive variables as

$$\mathbf{W}_0(x, \omega) = [\rho_0, u_0, p_0]^T = \begin{cases} [1.0, 0.0, 1.0] & \text{if } x < Y_1(\omega), \\ [0.125 + 0.5 Y_2, 0.0, 0.1] & \text{if } x > Y_1(\omega). \end{cases}$$

We apply the SFVM to solve the system (7.40)–(7.41) with  $Y_1(\omega) \sim \mathcal{U}[0.95, 1.05]$ ,  $Y_2(\omega) \sim \mathcal{U}[-0.1, 0.1]$ ,  $Y_3(\omega) \sim \mathcal{U}[1.2, 1.6]$  using the 3rd order WENO reconstruction in both physical and stochastic variables. The results are presented in Figs. 7.3–7.4, in which the solution mean (solid line) as well as mean plus/minus standard deviation (dashed lines) are plotted.

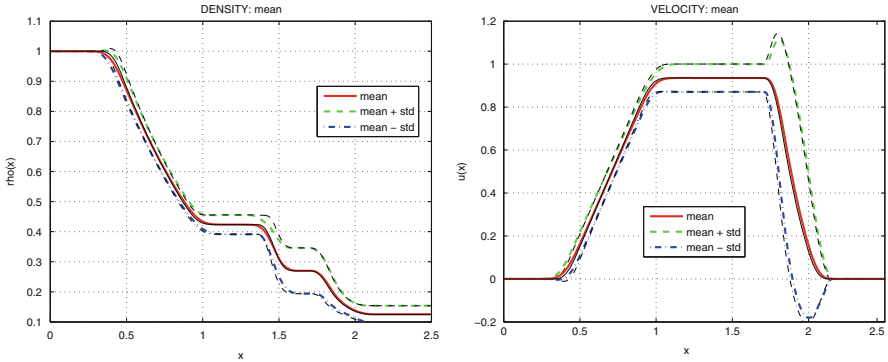


**Fig. 7.3** Sod’s shock tube problem with random flux and initial data: density (*left*) and velocity (*right*)

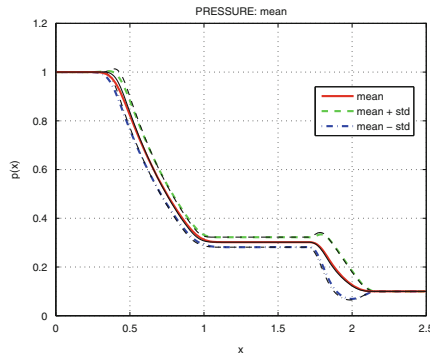


**Fig. 7.4** Sod’s shock tube problem with random flux and initial data: pressure

The convergence results (dependence of the error on the number of mesh points) for the solution mean are presented in Fig. 7.5. Due to the shock formation in the path-wise solution the maximum order of convergence for the mean is limited to 1st.

We compare the efficiencies of the SFV and MLMC methods [16, 17] for the solution of the one-dimensional stochastic Sod’s problem for the Euler equations. Figure 7.6 illustrates the convergence of SFVM and MLMC based on 1st and 2nd order FV ENO/WENO solvers.

Figure 7.6 demonstrates that both approaches lead to the same orders of convergence in space while SFVM with properly chosen reconstruction orders appears to be more efficient in terms of error-to-work estimates.

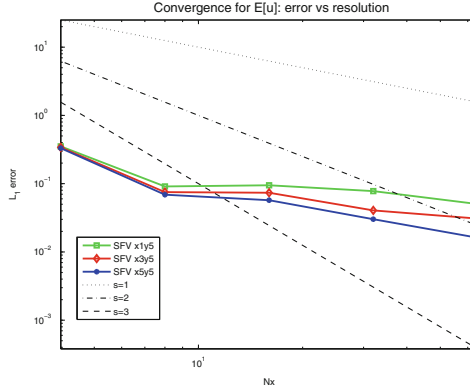


Fig. 7.5 Sod’s shock tube problem with random flux and initial data: convergence

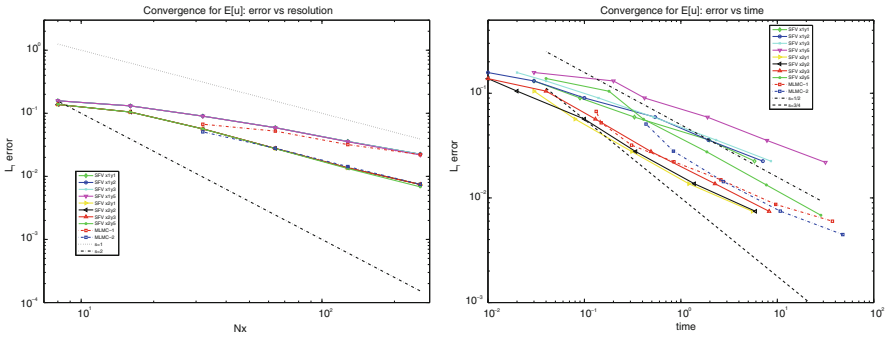


Fig. 7.6 Convergence of the SFVM and MLMC

7.4.4.2 Stochastic Cloud-Shock Interaction (Random IC)

Consider the two-dimensional Euler equations with random initial data:

$$\frac{\partial \mathbf{U}}{\partial t} + \frac{\partial \mathbf{F}(\mathbf{U})}{\partial x_1} + \frac{\partial \mathbf{G}(\mathbf{U})}{\partial x_2} = \mathbf{0}, \quad (x_1, x_2) \in [0, 1] \times [0, 1], \quad (7.42)$$

$$\mathbf{U}(x, 0, \omega) = \mathbf{U}_0(x, Y(\omega)), \quad (7.43)$$

where

$$\mathbf{U} = [\rho, \rho u, \rho v, E]^T,$$

$$\mathbf{F} = [\rho u, \rho u^2 + p, \rho uv, \rho u(E + p)]^T,$$

$$\mathbf{G} = [\rho u, \rho uv, \rho v^2 + p, \rho v(E + p)]^T,$$

$$p = (\gamma - 1) \left( E - \frac{1}{2} \rho (u^2 + v^2) \right).$$

We apply the SFV method to solve the stochastic shock-vortex interaction problem for the Euler equations (see [21] for the deterministic version of the problem). The initial Mach 1.1 shock wave is normal to the  $x_1$ -axis and has uncertain location at  $x_1 = 0.5 + 0.1Y(\omega)$  with  $Y(\omega) \sim \mathcal{U}[0, 1]$ . The states in front and behind the shock wave are:

$$[\rho_0, u_0, v_0, p_0] = \begin{cases} [1, \sqrt{\gamma}, 0, 1], & \text{if } x_1 < Y(\omega), \\ \left[ \frac{1}{1.1}, 1.1\sqrt{\gamma}, 0, 1 - \frac{\gamma}{10} \right], & \text{if } x_1 > Y(\omega). \end{cases}$$

A small vortex centered at  $(x_1^c, x_2^c) = (0.25, 0.5)$  is superposed to the flow left to the shock and is described as a perturbation to the velocity  $(u, v)$  and pressure  $p$ :

$$\begin{aligned} \tilde{u}_0 &= \epsilon \tau e^{\alpha(1-\tau^2)} \sin \theta, \\ \tilde{v}_0 &= -\epsilon \tau e^{\alpha(1-\tau^2)} \cos \theta, \\ \tilde{p}_0 &= -(\gamma - 1) \frac{\epsilon^2 e^{2\alpha(1-\tau^2)}}{4\alpha\gamma} \rho_0, \end{aligned}$$

where

$$r = \sqrt{(x_1 - x_1^c)^2 + (x_2 - x_2^c)^2}, \quad \tau = \frac{r}{r_c}, \quad \sin \theta = \frac{x_2 - x_2^c}{r}, \quad \cos \theta = \frac{x_1 - x_1^c}{r}.$$

Here  $\epsilon$  indicates the vortex strength,  $\alpha$  controls the decay rate of the vortex and  $r_c$  is the critical radius for which the vortex has the maximum strength. In our test we choose  $\epsilon = 0.3$ ,  $r_c = 0.05$  and  $\alpha = 0.204$ .

For this computation, we have used the SFV method based on 5th order WENO solver in the physical space and 2nd order ENO solver in the stochastic space on the uniform  $128 \times 128$  cells Cartesian grid in the physical space and 32 cells grid in the stochastic coordinate. The computational results for the flow mean and variance at  $t = 0.35$  are presented in Figs. 7.7–7.10.

## 7.5 Stochastic DG/FVM

### 7.5.1 Stochastic DG/FV Method

In this section we generalize the approach to uncertainty quantification described previously in order to efficiently apply high-order approximation techniques on

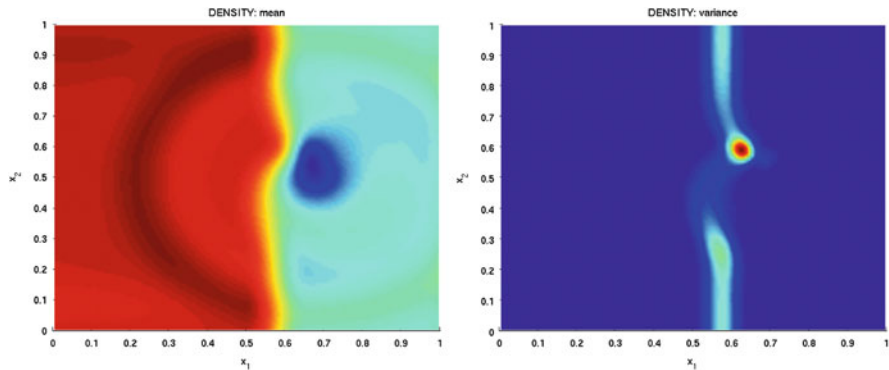


Fig. 7.7 Density: mean (left) and variance (right) at  $t = 0.35$

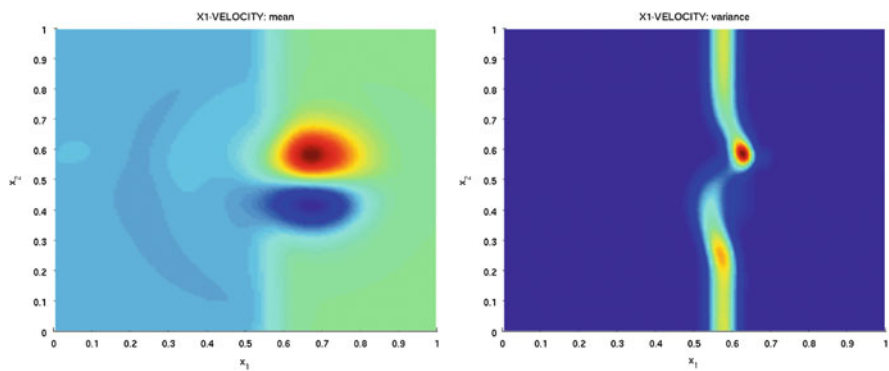


Fig. 7.8  $x_1$ -velocity: mean (left) and variance (right) at  $t = 0.35$

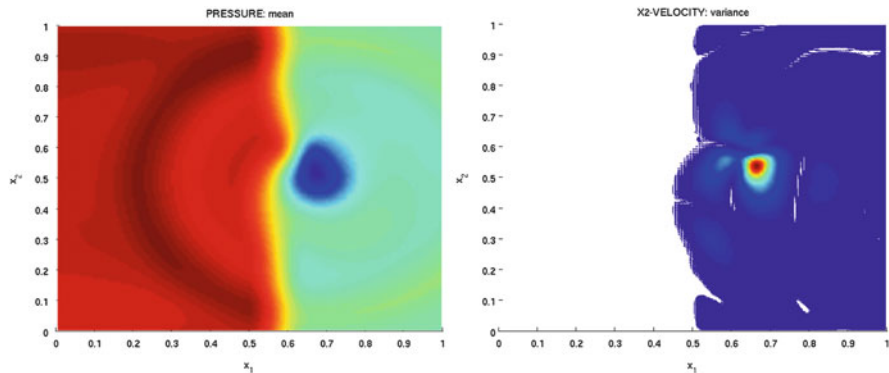
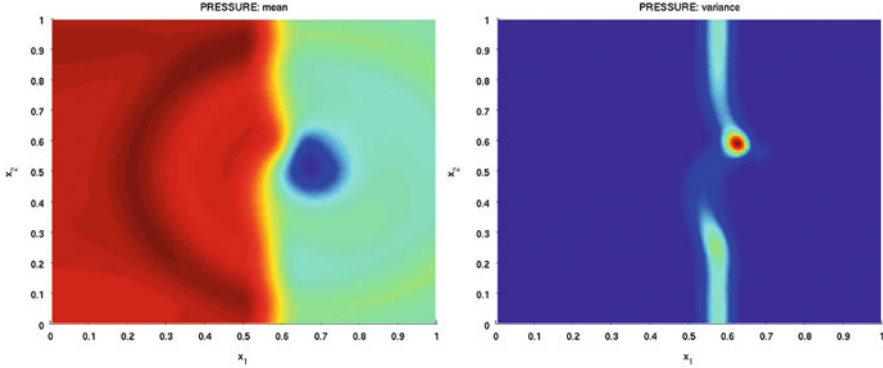


Fig. 7.9  $x_2$ -velocity: mean (left) and variance (right) at  $t = 0.35$





**Fig. 7.10** Pressure: mean (*left*) and variance (*right*) at  $t = 0.35$

unstructured grid in physical domains with complicated geometry. To this end, we use the Discontinuous Galerkin (DG) method [4] to discretize the equations in the physical space and combine it with the finite-volume discretization in the stochastic variables as described in Sect. 7.3. Note that we can still use Cartesian grids in the stochastic space since the computational domain in this space is a  $q$ -dimensional rectangle.

As before, we start with the parametric form of the stochastic conservation law:

$$\partial_t \mathbf{U} + \nabla_x \cdot \mathbf{F}(\mathbf{U}, \mathbf{y}) = \mathbf{0}, \quad \mathbf{x} \in D_x \subset \mathbb{R}^3, \quad \mathbf{y} \in D_y \subset \mathbb{R}^q, \quad t > 0; \quad (7.44)$$

$$\mathbf{U}(\mathbf{x}, 0, \mathbf{y}) = \mathbf{U}_0(\mathbf{x}, \mathbf{y}), \quad \mathbf{x} \in D_x \subset \mathbb{R}^3, \quad \mathbf{y} \in D_y \subset \mathbb{R}^q. \quad (7.45)$$

On each element  $K_x^i$  of the physical domain triangulation we apply the DG solution discretization in the physical variable  $\mathbf{x}$ :

$$\mathbf{U}_h(\mathbf{x}, t, \mathbf{y}) = \sum_{l=1}^p \mathbf{U}_l(t, \mathbf{y}) \varphi_l(\mathbf{x}), \quad \mathbf{x} \in K_x^i, \quad (7.46)$$

which leads to the following semi-discrete DG formulation:

$$\sum_{l=1}^p \partial_t \mathbf{U}_l(t, \mathbf{y}) \int_{K_x^i} \varphi_l(\mathbf{x}) \varphi_k(\mathbf{x}) d\mathbf{x} + \int_{\partial K_x^i} \mathbf{F}(\mathbf{U}_h, \mathbf{y}) \cdot \mathbf{n} \varphi_k(\mathbf{x}) d\mathbf{x} - \int_{K_x^i} \mathbf{F}(\mathbf{U}_h, \mathbf{y}) \nabla \varphi_k(\mathbf{x}) d\mathbf{x} = \mathbf{0}. \quad (7.47)$$

Note that at this stage the DG coefficients are still functions of the random variable  $\mathbf{y}$  and time  $t$  and thus to get rid of this dependence we apply the finite-volume discretization in the random variable, which leads to

$$\begin{aligned} & \sum_{l=1}^p \int_{K_y^j} \left[ \partial_t \mathbf{U}_l(t, \mathbf{y}) \int_{K_x^i} \varphi_l(\mathbf{x}) \varphi_k(\mathbf{x}) d\mathbf{x} \right] \mu(\mathbf{y}) d\mathbf{y} + \\ & + \int_{K_y^j} \left[ \int_{\partial K_x^i} \mathbf{F}(\mathbf{U}_h, \mathbf{y}) \cdot \mathbf{n} \varphi_k(\mathbf{x}) d\mathbf{x} \right] \mu(\mathbf{y}) d\mathbf{y} - \\ & - \int_{K_y^j} \left[ \int_{K_x^i} \mathbf{F}(\mathbf{U}_h, \mathbf{y}) \nabla \varphi_k(\mathbf{x}) d\mathbf{x} \right] \mu(\mathbf{y}) d\mathbf{y} = \mathbf{0}. \quad (7.48) \end{aligned}$$

Finally, the resulting scheme becomes

$$\begin{aligned} & \sum_{l=1}^p \frac{d\mathbf{U}_{lk}(t)}{dt} \int_{K_x^i} \varphi_l(\mathbf{x}) \varphi_k(\mathbf{x}) d\mathbf{x} + \frac{1}{|K_y^j|} \iint_{K_y^j \partial K_x^i} \mathbf{F}(\mathbf{U}_h, \mathbf{y}) \cdot \mathbf{n} \varphi_k(\mathbf{x}) \mu(\mathbf{y}) d\mathbf{x} d\mathbf{y} - \\ & - \frac{1}{|K_y^j|} \iint_{K_y^j K_x^i} \mathbf{F}(\mathbf{U}_h, \mathbf{y}) \nabla \varphi_k(\mathbf{x}) \mu(\mathbf{y}) d\mathbf{x} d\mathbf{y} = \mathbf{0}, \quad (7.49) \end{aligned}$$

which is an ODE system with respect to the DG coefficients averaged over an element of the stochastic grid.

## 7.5.2 Numerical Results

### 7.5.2.1 Stochastic Cloud-Shock Interaction Problem (Random Flux)

Consider the two-dimensional Euler equations with deterministic initial data

$$[\rho_0, u_0, v_0, p_0] = \begin{cases} [3.86859, 11.2536, 0, 167.345], & \text{if } x_1 < 0.05, \\ [1, 0, 0, 1], & \text{if } x_1 > 0.05, \end{cases}$$

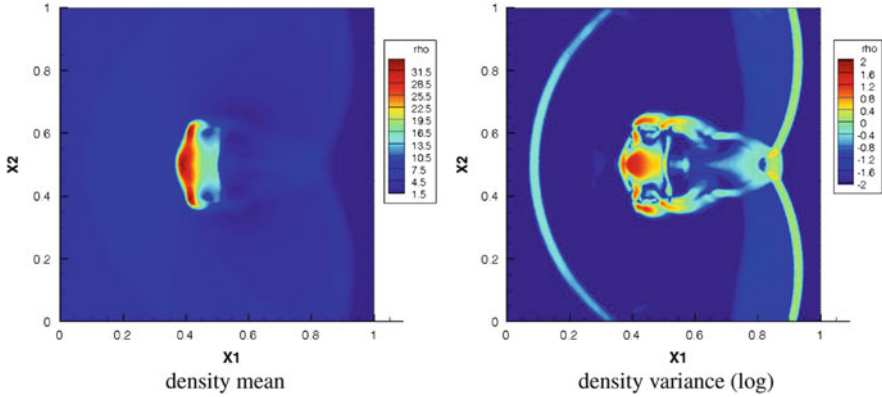


**Fig. 7.11** Stochastic cloud-shock interaction problem

and a high-density cloud lying to the right of the shock:

$$\rho_0 = 10, \text{ if } \sqrt{(x_1 - 0.25)^2 + (x_2 - 0.5)^2} \leq 0.15.$$

Assume the random  $\gamma = \gamma(\omega)$  in the equation of state (EOS)

$$p = (\gamma(\omega) - 1) \left( E - \frac{1}{2} \rho (u^2 + v^2) \right),$$

$$\gamma(\omega) \sim \mathcal{U}(5/3 - \epsilon, 5/3 + \epsilon), \quad \epsilon = 0.1$$

The results of the simulation are presented in Fig. 7.11. In our computations we have used the 2nd order DG method in  $\mathbf{x}$  variable and 3rd order WENO method in  $\mathbf{y}$  variable, triangular mesh in  $\mathbf{x}$  consisting of about 170,000 cells and Cartesian mesh in  $\mathbf{y}$  consisting of 16 cells. The results are plotted at  $T = 0.06$ .

### 7.5.2.2 Forward-Facing Step Channel

Consider the stochastic flow in the channel with the forward facing step with random Mach number of the inflowing gas:  $M \sim \mathcal{U}(2.9, 3.1)$ . We have used the mesh of about 13,000 triangular cells in the physical space and 15 equally-sized cells in the stochastic space, the methods used are 2nd order DG and 3rd order WENO in physical and random variables, respectively. The results of the simulation are given in Fig. 7.12, indicating that the uncertainty in the Mach number influences the position and intensity of shock in front of the step, while having little effect on the shocks reflected from the channel walls.

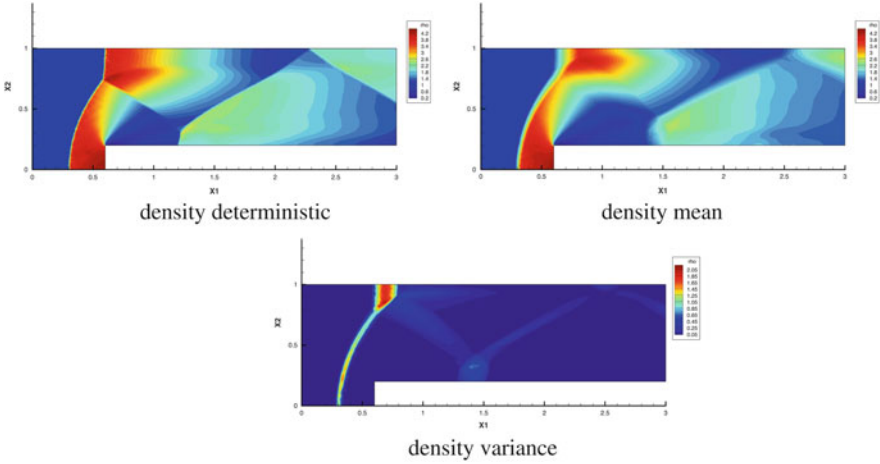


**Fig. 7.12** Stochastic flow in a forward-facing step channel

## 7.6 Stochastic Mesh Adaptation

### 7.6.1 Stochastic Mesh Adaptation Based on Karhunen-Loève Expansion

In this section we discuss one mesh adaptation technique which can be used to reduce the computational cost of the SFV method. To this end, we consider the following model problem:

$$\frac{\partial u}{\partial t} + \frac{\partial f(u, \omega)}{\partial x} = 0, \quad x \in D = [0, L] \subset \mathbb{R}, \quad t > 0; \quad (7.50)$$

$$u(x, 0, \omega) = u_0(x, \omega), \quad x \in D, \quad \omega \in \Omega. \quad (7.51)$$

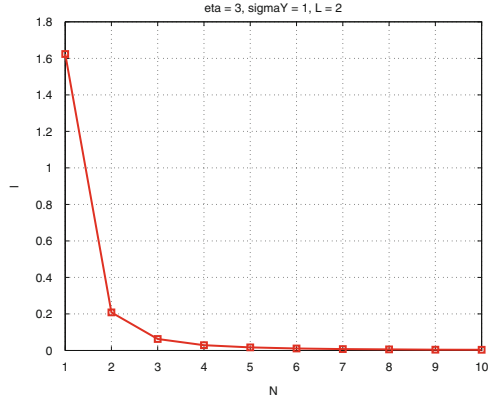
Assume the following Karhunen-Loève expansion of the flux:

$$f(u; \omega) = \bar{f}(u) + \sum_{j \geq 1} Y_j(\omega) \sqrt{\lambda_j} \Phi_j(u), \quad (7.52)$$

where  $\Phi_j(u)$  and  $\lambda_j$  are the eigenfunctions and eigenvalues of the integral operator with covariance kernel:

$$\int_D C_Y(u_1, u_2) \Phi(u_1) du_1 = \lambda \Phi(u_2).$$

**Fig. 7.13** Eigenvalues



We can therefore choose the random variable to parametrize the stochastic conservation law as  $\mathbf{y} = (y_1, y_2, \dots) = \mathbf{Y}(\omega) = (Y_1(\omega), Y_2(\omega), \dots)$ , then

$$f(u; \omega) = f(u; \mathbf{y}) \Big|_{\mathbf{y}=\mathbf{Y}(\omega)} = \frac{u^2}{2} + \delta \left( \sum_{j=1}^q y_j \sqrt{\lambda_j} \Phi_j(u) \right).$$

Let  $f(u; \omega)$  be the Gaussian process with exponential covariance [6]

$$C_Y(u_1, u_2) = \sigma_Y^2 e^{-|u_1 - u_2|/\eta}, \quad \text{then}$$

$$\lambda_j = \frac{2\eta\sigma_Y^2}{\eta^2 w_j^2 + 1}, \quad \Phi_j(u) = \frac{1}{\sqrt{(\eta^2 w_j^2 + 1)L/2 + \eta}} [\eta w_j \cos(w_j u) + \sin(w_j u)],$$

where  $w_j$  are the roots of

$$(\eta^2 w^2 - 1) \sin(wL) = 2\eta w \cos(wL)$$

and

$$Y_j \sim \mathcal{N}(0, 1), \quad \mathbb{E}[Y_j Y_k] = \delta_{jk}$$

Note that in this case the coefficients  $\lambda_j$  decay quickly in  $j$  (see Fig. 7.13).

Therefore the KL expansion can be truncated at moderate number of terms ( $q = 2, 3$ ) without losing too much information about the stochastic process, namely

$$f(u; \mathbf{y}) = \bar{f}(u) + \sum_{j=1}^q y_j \sqrt{\lambda_j} \Phi_j(u)$$

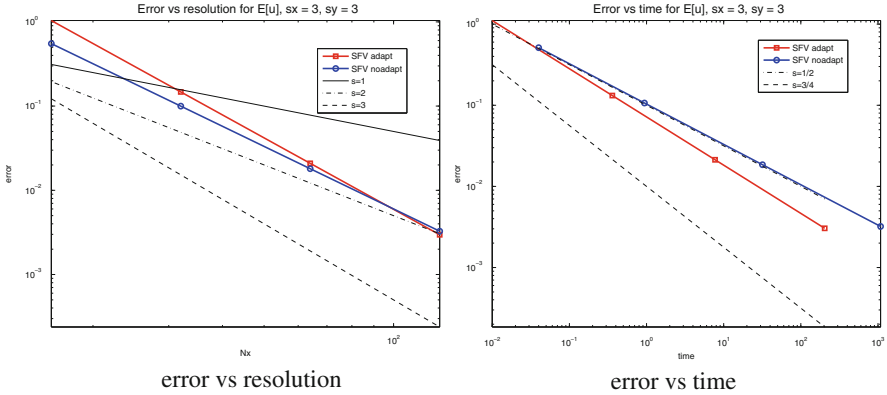


**Fig. 7.14** Convergence of the SFVM: adaptive (*squares*) va. non-adaptive (*circles*) mesh

Consider the stochastic SCL with random flux and deterministic initial data

$$u_t + f(u; \omega)_x = 0, \quad x \in (0, L), \quad t > 0, \tag{7.53}$$

$$u(x, 0; \omega) = u_0(x) = 1 + \sin(\pi x). \tag{7.54}$$

In this paper, in order to reduce the computational cost of the SFV method, we propose the mesh adaptation in the stochastic space based on the choice of the number of nodes in each of the stochastic coordinates according to

$$N_y^j = C N_x \sqrt{\lambda_j}. \tag{7.55}$$

Figure 7.14 shows the convergence of the adaptive SFVM algorithm (“SFV adapt”) and the SFVM without stochastic mesh adaptation (“SFV noadapt”). The non-adaptive version of the SFVM simply uses equal number of cells in each stochastic coordinate, while the adaptive version chooses the number of cells in each  $y_j$  according to (7.55). The computational time needed to perform both algorithms is shown in Fig. 7.15. Clearly, the proposed adaptation of the algorithm improves the convergence properties of the SFV method.

## 7.6.2 Numerical Results

### 7.6.2.1 Stochastic Cloud-Shock Interaction Problem (Random IC)

We use the mesh adaptation approach similar to the one described above to solve the stochastic cloud-shock interaction problem with initial data depending on *four* random variables. Note that the usage of non-adaptive algorithm for such simulation would lead to excessive computational cost of SFVM.

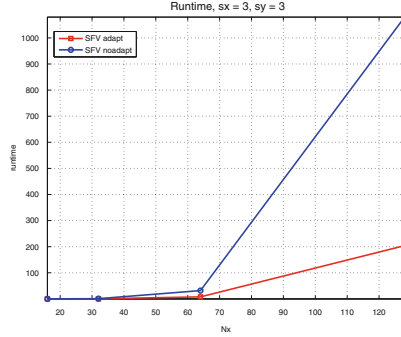


Fig. 7.15 Computational time: adaptive (squares) vs. non-adaptive (circles) mesh

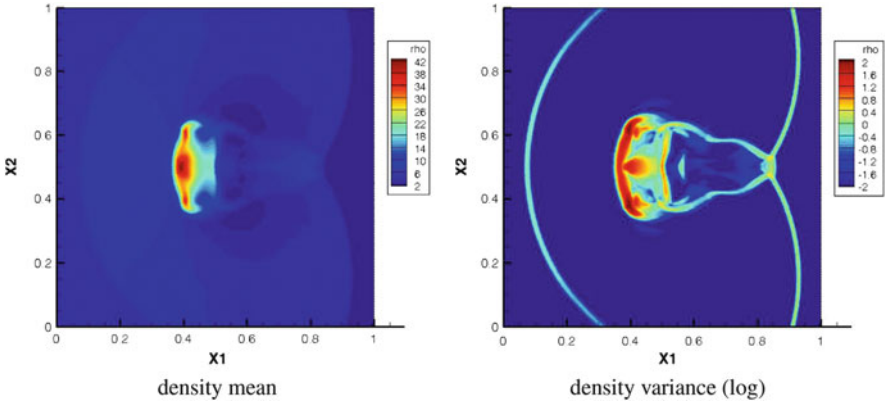


Fig. 7.16 Stochastic cloud-shock interaction problem

Consider the two-dimensional Euler equations with deterministic initial data

$$\mathbf{W}_0 = \begin{cases} [3.86859 + 0.1Y_2(\omega), 11.2536, 0, 167.345], & \text{if } x_1 < 0.04 + 0.01Y_1(\omega), \\ [1, 0, 0, 1], & \text{if } x_1 > 0.04 + 0.01Y_1(\omega), \end{cases}$$

with a high-density cloud to the right of the shock:

$$\rho_0 = 10 + 0.5Y_3(\omega), \text{ if } \sqrt{(x_1 - 0.25)^2 + (x_2 - 0.5)^2} \leq 0.15 + 0.02Y_4(\omega).$$

The equations are closed by the following deterministic EOS:  $p = (\gamma - 1)\left(E - \frac{1}{2}\rho(u^2 + v^2)\right)$ ,  $\gamma = 5/3$ . The random variables in the initial condition are uniformly distributed on  $[0, 1]$ :  $Y_k \sim \mathcal{U}[0, 1]$ ,  $k = 1, \dots, 4$ .

We use the 2nd order DG in  $\mathbf{x}$  variable and 3rd order WENO in  $\mathbf{y}$  variable, triangular mesh in  $\mathbf{x}$  (170,000 cells) and *adaptive* Cartesian mesh in  $\mathbf{y}$  ( $3 \cdot 2 \cdot 7 \cdot 11 = 462$  cells), the output time is  $T = 0.06$ . The results of this simulation are illustrated in Fig. 7.16.

## 7.7 Conclusions

The SFV and SDG/FV methods studied in this paper appear to be a flexible and effective approach to the solution of stochastic conservation laws. We have shown that the SFV method it is applicable for the uncertainty quantification in a variety of complex problems including systems of conservation laws with random flux coefficients and initial data with several sources of uncertainty. The proper adaptation of the stochastic grid significantly reduces the computational cost of the method and improves its convergence.

## References

1. Abgrall, R.: A simple, flexible and generic deterministic approach to uncertainty quantification in non-linear problems. Rapport de Recherche, INRIA, 00325315 (2007)
2. Abgrall, R., Congedo, P.M.: A sem-intrusive deterministic approach to uncertainty quantification in non-linear fluid flow problems. *J. Comput. Phys.* **235**, 828–845 (2013)
3. Barth, T.: On the propagation of the statistical model parameter uncertainty in CFD calculations. *Theor. Comput. Fluid Dyn.* (2011). doi:10.1007/s00162-011-0221-2
4. Cockburn, B., Shu, C.W.: The Runge-Kutta discontinuous Galerkin method for conservation laws V: multidimensional systems. *J. Comput. Phys.* **141**, 199–224 (1998)
5. Debusschere, B., Najm, H., Pébay, P., Knio, O., Ghanem, R., Le Maître, O.: Numerical challenges in the use of polynomial chaos representations for stochastic processes. *SIAM J. Sci. Comput.* **26**, 698–719 (2004)
6. Ghanem, R., Spanos, P.: *Stochastic Finite Elements: A Spectral Approach*. Dover, Mineola (2003)
7. Godlewski, E., Raviart, P.: *Hyperbolic Systems of Conservation Laws*. Ellipses Publishing, Paris (1995)
8. Gottlieb, D., Xiu, D.: Galerkin method for wave equations with uncertain coefficients. *Commun. Comput. Phys.* **3**, 505–518 (2008)
9. Knio, O., Le Maître, O.: Uncertainty propagation in CFD using polynomial chaos decomposition. *Fluid Dyn. Res.* **38**, 616–640 (2006)
10. Le Maître, O., Knio, O., Najm, H., Ghanem, R.: Uncertainty propagation using Wiener-Haar expansions. *J. Comput. Phys.* **197**, 28–57 (2004)
11. Le Maître, O., Najm, H., Ghanem, R., Knio, O.: Multi-resolution analysis of Wiener-type uncertainty propagation schemes. *J. Comput. Phys.* **197**, 502–531 (2004)
12. Le Maître, O., Najm, H., Pébay, P., Ghanem, R., Knio, O.: Multi-resolution analysis scheme for uncertainty quantification in chemical systems. *SIAM J. Sci. Comput.* **29**, 864–889 (2007)
13. LeVeque, R.: *Numerical Methods for Conservation Laws*. Birkhäuser Verlag, Basel/Boston (1992)
14. Lin, G., Su, C.-H., Karniadakis, G.E.: Predicting shock dynamics in the presence of uncertainties. *J. Comput. Phys.* **217**, 260–276 (2006)
15. Lin, G., Su, C.-H., Karniadakis, G.E.: Stochastic modelling of random roughness in shock scattering problems: theory and simulations. *Comput. Methods Appl. Mech. Eng.* **197**, 3420–3434 (2008)
16. Mishra, S., Schwab, Ch.: Sparse tensor multi-level Monte Carlo finite volume methods for hyperbolic conservation laws with random initial data. *Math. Comput.* **81**, 1979–2018 (2012)
17. Mishra, S., Schwab, Ch., Šukys, J.: Multi-level Monte Carlo finite volume methods for nonlinear systems of conservation laws in multi-dimensions. *J. Comput. Phys.* **231**, 3365–3388 (2012)



18. Mishra, S., Risebro, N.H., Schwab, Ch., Tokareva, S.: Numerical solution of scalar conservation laws with random flux functions. SAM report 2012-35. <http://www.sam.math.ethz.ch/reports/2012/35>
19. Poëtte, G., Després, B., Lucor, D.: Uncertainty quantification for systems of conservation laws. *J. Comput. Phys.* **228**, 2443–2467 (2009)
20. Schwab, Ch., Tokareva, S.: High order approximation of probabilistic shock profiles in hyperbolic conservation laws with uncertain initial data. *ESAIM M2AN* **47**, 807–835 (2013)
21. Shu, C.W.: High order ENO and WENO schemes for computational fluid dynamics. In: Barth, T.J., Deconinck, H. (eds.) *High-Order Methods for Computational Physics*. Springer, Berlin/New York (1999)
22. Troyen, J., Le Maître, O., Ndjinga, M., Ern, A.: Intrusive Galerkin methods with upwinding for uncertain nonlinear hyperbolic systems. *J. Comput. Phys.* **229**, 6485–6511 (2010)
23. Troyen, J., Le Maître, O., Ndjinga, M., Ern, A.: Roe solver with entropy corrector for uncertain hyperbolic systems. *J. Comput. Phys.* **235**, 491–506 (2010)
24. Wan, X., Karniadakis, G.E.: Multi-element generalized polynomial chaos for arbitrary probability measures. *SIAM J. Sci. Comput.* **28**, 901–928 (2006)
25. Xiu, D., Karniadakis, G.E.: Modeling uncertainty in steady state diffusion problems via generalized polynomial chaos. *Comput. Methods Appl. Mech. Eng.* **191**, 4927–4948 (2002)
26. Xiu, D., Karniadakis, G.E.: Modeling uncertainty in flow simulations via generalized polynomial chaos. *J. Comput. Phys.* **187**, 137–167 (2003)